


Article

Gold-Based Catalysts for Complete Formaldehyde Oxidation: Insights into the Role of Support Composition

Lyuba Ilieva ¹, Dimitar Dimitrov ², Elitsa Kolentsova ², Anna Maria Venezia ³ , Daniela Karashanova ⁴ , Georgi Avdeev ⁵, Petya Petrova ¹, Razvan State ⁶ and Tatyana Tabakova ^{1,*} 

¹ Institute of Catalysis, Bulgarian Academy of Sciences, 1113 Sofia, Bulgaria; luliieva@ic.bas.bg (L.I.); petia@ic.bas.bg (P.P.)

² Department of Chemistry and Phytopharmacy, Agricultural University, 4000 Plovdiv, Bulgaria; mitko_dme@abv.bg (D.D.); elitsa_kolentsova@abv.bg (E.K.)

³ Istituto per lo Studio dei Materiali Nanostrutturati, Consiglio Nazionale delle Ricerche (CNR), 90146 Palermo, Italy; annamaria.venezia@cnr.it

⁴ Institute of Optical Materials and Technologies, Bulgarian Academy of Sciences, 1113 Sofia, Bulgaria; dkarashanova@yahoo.com

⁵ Institute of Physical Chemistry, Bulgarian Academy of Sciences, 1113 Sofia, Bulgaria; g_avdeev@abv.bg

⁶ "Ilie Murgulescu" Institute of Physical Chemistry, Romanian Academy, 060021 Bucharest, Romania; rstate@icf.ro

* Correspondence: tabakova@ic.bas.bg



Citation: Ilieva, L.; Dimitrov, D.; Kolentsova, E.; Venezia, A.M.; Karashanova, D.; Avdeev, G.; Petrova, P.; State, R.; Tabakova, T. Gold-Based Catalysts for Complete Formaldehyde Oxidation: Insights into the Role of Support Composition. *Catalysts* **2022**, *12*, 705. <https://doi.org/10.3390/catal12070705>

Academic Editors: Salvatore Scirè and Leonarda Francesca Liotta

Received: 27 May 2022

Accepted: 24 June 2022

Published: 27 June 2022

Publisher's Note: MDPI stays neutral with regard to jurisdictional claims in published maps and institutional affiliations.



Copyright: © 2022 by the authors. Licensee MDPI, Basel, Switzerland. This article is an open access article distributed under the terms and conditions of the Creative Commons Attribution (CC BY) license (<https://creativecommons.org/licenses/by/4.0/>).

Abstract: Formaldehyde (HCHO) is recognized as one of the most emitted indoor air pollutants with high detrimental effect on human health. Significant research efforts are focused on HCHO removal to meet emission regulations in an effective and economically profitable way. For over three decades, the unique electronic properties and catalytic abilities of nano-gold catalysts continue to be an attractive research area for the catalytic community. Recently, we reported that mechanochemical mixing is a relevant approach to the preparation of Co-Ce mixed oxides with high activity in complete benzene oxidation. A trend of higher surface defectiveness, in particular, oxygen vacancies, caused by close interaction between cobalt oxide and cerium oxide phases, was observed for a mixed oxide composition of 70 wt.% Co₃O₄ and 30 wt.% CeO₂. These results directed further improvement by promotion with gold and optimization of mixed oxide composition, aiming for the development of an efficient catalyst for room temperature HCHO abatement. Support modification with potassium was studied; however, the K addition caused less enhancement of HCHO oxidation activity than expected. This motivated the preparation of new carrier material. In addition to Co₃O₄-CeO₂ mixed metal oxides with preset ratio, γ -Al₂O₃ intentionally containing 33% boehmite and shortly named Al₂O₃-b was used for synthesis. Analysis of the role of support composition in HCHO oxidation was based on the characterization of nano-gold catalysts by textural measurements, XRD, HRTEM, XPS, and TPR techniques. Gold supported on mechanochemically treated Co₃O₄-CeO₂-Al₂O₃-b (50 wt.% Al₂O₃-b) exhibited superior activity owing to high Ce³⁺ and Co³⁺ surface amounts and the most abundant oxygen containing species with enhanced mobility. This catalyst achieved oxidation to CO₂ and H₂O by 95% HCHO conversion at room temperature and 100% at 40 °C, thus implying the potential of this composition in developing efficient catalytic materials for indoor air purification.

Keywords: gold catalysts; HCHO oxidation; Co₃O₄-CeO₂ mixed oxides; mechanochemical preparation; potassium modification

1. Introduction

Formaldehyde (HCHO) is toxic and very dangerous with established carcinogenic effect during prolonged exposure. HCHO is one of the most dominant indoor air pollutants originated mainly from building, furniture, decorative, and other artificial materials, household goods, and indoor smoking. These are sources that are difficult to avoid, and

many efforts are focused on formaldehyde abatement to the required concentration levels. As an outdoor pollutant, formaldehyde is also present in the exhaust of diesel engines. An efficient, cost-effective, and environmentally friendly approach for its elimination is the complete HCHO oxidation to H₂O and harmless CO₂ with a lack of unfavorable side products. Recently, research progress in catalytic HCHO oxidation using transition metal oxide-based and noble metal-based catalysts has been a subject of review [1–3]. Newly, Li and coauthors [4] summarized the results of Co₃O₄-containing materials for the catalytic oxidation of formaldehyde. Besides a discussion on physical and chemical properties of the catalysts, the authors focused attention on the experimental conditions during catalytic tests, in particular, humidity and the effect of water concentration, revealing also some aspects of reaction mechanism. Low cost and highly stable Co₃O₄ catalysts exhibit moderately low-temperature catalytic activity in complete HCHO oxidation but still the best results of total formaldehyde combustion have not reached levels below 80–90 °C. Many preparation methods, including template and surfactant utilization, were applied to the design and investigation of HCHO oxidation over Co₃O₄ of various particle size, morphology, and crystal face exposure determined by structural differences: two- or three-dimensional ordered mesoporous (2D or 3D) Co₃O₄ [5,6], Co₃O₄ nanofibers [7], nanowires [8], nanobelts, nanoplates, and nanosheets [9]. Variation of catalyst physical and chemical features was also achieved by changing process conditions of synthesis or calcination [4] (and references therein) [10]. Textural properties, such as specific surface area, average pore volume, and pore diameter, are very important for providing more active sites for adsorption and reaction [11,12]; however, the structure of the catalyst surface plays a crucial role for formaldehyde oxidation activity.

Many researchers have been focused on improving catalytic behavior by combination between Co₃O₄ and other appropriate metal oxides. Various chemical compositions have been studied, including transition metals, such as widely used Ce and Mn [4] (and references therein), Ni [13], Zn [14,15], and Cr [15,16]. Significant temperature lowering in complete formaldehyde oxidation was shown in the presence of supported noble metals. Li et al. [4] (and references therein) demonstrated the role of Pt, Au, and Ag on Co₃O₄ and Co₃O₄/transition-metal oxides composites. It was reported that the HCHO conversion over different catalytic systems could be promoted by the presence of alkali metal ions, and such modification was beneficial in the case of Co₃O₄-based catalysts as well. Bai and Li [17] reported a promotional effect of K⁺ ion on the activity of Ag/Co₃O₄. Using various precipitants for Co₃O₄ preparation, Fan et al. showed that KHCO₃ is the most promising one. These authors claimed that one of the reasons for higher activity in the oxidation of HCHO was related to the presence of residual K⁺ ions because alkaline hydrolysis may accelerate oxidation [18]. Later, Fan and coauthors [19] used Co₃O₄ impregnation with K₂CO₃, KNO₃, and KCl salts. The highest promotional effect on HCHO oxidation was achieved by means of K₂CO₃ with an optimal concentration of 3 wt.% and explained by increased Co³⁺/Co²⁺ surface ratio and surface oxygen vacancy formation as well as by the role of generated OH groups to enhance oxidation of intermediate species. However, contrary to these results of HCHO oxidation, in a study of total CO and propane oxidation over Co₃O₄ nanocatalysts, Tang et al. [20] reported a “locking-effect” of oxygen, leading to poor oxygen mobility of alkali metal doped Co₃O₄ catalysts with an additional poisoning effect related to the enhanced adsorption of CO₂ and robust surface carbonate species formation.

Currently, gold-based catalysts are of considerable interest. Depending on various factors determining gold particle size and support features, the positive effect of gold on the catalytic activity in many reactions, in particular, the complete oxidation of VOCs, is already clearly documented [21,22]. Ceria's unique redox properties and ability to provide high dispersion of supported metals has been widely investigated as suitable carrier of gold catalysts. In a recent review, Gaálová and Topka [23] summarized published results for gold and ceria as catalysts for VOCs abatement, paying attention to optimal gold particle size and gold/ceria interface as main factors for enhanced activity and/or selectivity. DFT calculations confirmed the observed significant impact of oxygen vacancy concentration,

showing that the gold containing defective Au/CeO₂ (111) surface with multiple oxygen vacancies is more favorable for formaldehyde adsorption and oxidation [24].

Deposition of gold could significantly promote catalytic activity, but this effect is associated with small Au particles. Liu et al. [25] commented the problem of Au particle agglomeration upon loading on pristine Co₃O₄ by the deposition–precipitation method. Low-temperature HCHO oxidation over gold catalysts on mixed CeO₂-Co₃O₄ supports brings about expected benefits. Besides the textural, morphological, and structural dependences, the catalytic behavior is influenced by mixed metal oxide composition. Different opinions are encountered in the literature concerned with favorable Ce/Co atomic ratio for the interaction between gold, CeO₂, and Co₃O₄. In a study of CeO₂-Co₃O₄ of variable Co/(Co+Ce) atomic ratio prepared by the sol-gel method, Lu et al. [26] established the highest CeO₂-Co₃O₄ reducibility and catalytic performance for a Co/(Co+Ce) ratio value of 0.95. In this case, complete oxidation of HCHO was attained at 80 °C. Ma et al. [5] compared 2D Au/Co₃O₄ and 2D Au/Co₃O₄-CeO₂ for room-temperature formaldehyde elimination. Au/Co₃O₄ exhibited the highest activity, and a decrease in activity was observed on increasing CeO₂ content. Liu and coworkers found a superior HCHO oxidation activity of gold on 3D ordered macroporous (3DOM) CeO₂-Co₃O₄ as compared to Au/CeO₂ and Au/Co₃O₄ matching catalysts. A beneficial role of the interaction between Co₃O₄ and CeO₂ for oxygen transfer during the HCHO oxidation was proposed. The catalytic activity was strongly dependent on the Ce/Co molar ratio, and total HCHO elimination at 39 °C was achieved over a sample with optimal composition of 3 wt.% gold and Ce/Co molar ratio of 2.5:1 [25]. Qu et al. proved the best performance of 3D Au-Ce_xCo_y catalysts of different CeO₂ to Co₃O₄ ratio for a composition containing 3 wt.% Au on Ce₃Co to be 3:1. Facilitated HCHO oxidation was related to synergistic effect between CeO₂ and Co₃O₄, which promotes the migration of oxygen species and Au activation. Supplemental improvement of catalytic performance (100% conversion at 60 °C) was accomplished using graphene oxide aerogel [27]. Recently, Rochard and coworkers [28] established a remarkable increase in HCHO conversion at ambient temperature using 3 wt.% gold deposited on Co-promoted ceria (9 mol.%). The catalytic properties were commented in line with created higher concentration of oxygen vacancies for better redox properties and better oxidation activity associated with enhanced oxygen activation and oxygen mobility.

The interest of the present study is directed toward formaldehyde complete oxidation over supported gold catalysts. Undoubtedly, a small amount of added gold makes the catalyst somewhat cost ineffective; however, this could be less significant than substantial enhancement of the catalytic performance. The chosen carrier for gold deposition was a mechanochemically synthesized mixed oxide containing 70 wt.% Co₃O₄ and 30 wt.% CeO₂. The selection of this composition was made based on the best activity of the aforementioned catalytic material manifested in complete benzene oxidation [29]. K⁺ doping effect on HCHO oxidation activity was also evaluated. To the best of our knowledge, the gold promotion of the Co₃O₄-CeO₂ mixed oxide carrier prepared by the less polluting, less energy demanding, less hazardous, and simple mechanochemical method has not been studied in the HCHO oxidation reaction. The role of K⁺ on HCHO oxidation over Au/Co₃O₄-CeO₂ catalysts has not been reported either.

The overarching aim to develop highly efficient but also economically viable catalysts motivated the authors for further synthesis of a new support by reducing the active component amount, e.g., through decreasing the Co-Ce mixed oxide content. In view of the expected positive role of hydroxyl groups in contributing to enhanced HCHO oxidation, the support was mechanochemically prepared from a mixture of the selected Co-Ce composition and low cost γ -Al₂O₃ containing boehmite (γ -AlOOH) on purpose. The latter is characterized by a high surface area and high density of surface OH groups. A literature survey revealed that such a type of carrier is not used to prepare gold-based catalysts. The superior activity of the resultant supported gold catalyst is discussed.

2. Results and Discussion

2.1. Catalytic Activity in HCHO Oxidation

Catalytic tests in the reaction of HCHO oxidation performed at gas hourly space velocities (GHSV) of 10,000 and then repeated at 20,000 h⁻¹ showed stable work with the same catalytic behavior. Figure 1 depicts the catalytic activity (GHSV = 20,000 h⁻¹) expressed as degree of HCHO conversion over undoped, K-doped Co-Ce mixed oxides, and supported gold catalysts. Products of incomplete oxidation were not registered. Potassium addition led to improved performance of Co-Ce+K as compared to Co-Ce mixed oxide; however, the 100% HCHO conversion over both supports was achieved at about the same temperature of 150 °C. Gold loading provoked very significant enhancement of HCHO oxidation activity throughout the low temperature range and especially at room temperature but complete HCHO conversion over Au/Co-Ce catalyst was reached at still high temperature of 100 °C. The following order of activities was observed comparing with gold supported on bare oxides: Au/Co-Ce > Au/Ce > Au/Co within investigated temperature and in particular at room temperature, at which the HCHO conversion was 80% over Au/Co-Ce, 59% over Au/Ce, and below 10% over Au/Co (Figure S1). Ma et al. prepared Co₃O₄, CeO₂, and Co₃O₄-CeO₂ supported Au catalysts with a 2D structure and reported that the 2D Au/Co₃O₄ catalyst exhibited higher HCHO oxidation activity than the Au/Co₃O₄-CeO₂ and Au/CeO₂ catalysts by supposing a higher intrinsic activity of Co₃O₄ than that of CeO₂ [5]. However, like in this study, among gold on 3DOM Co₃O₄, CeO₂, and Co₃O₄-CeO₂, Au/Co₃O₄-CeO₂ manifested a higher activity than Au/CeO₂, while Au/Co₃O₄ demonstrated the lowest activity [25]. The present much higher catalytic activity of gold on a mixed metal oxide as compared to gold on single metal oxides should be related to the beneficial role of close interaction between Co₃O₄ and CeO₂ phases as induced by mechanochemical treatment.

The catalytic activity in HCHO oxidation over Au/Co-Ce+K was only slightly higher than that of Au/Co-Ce catalyst, and no temperature lowering at complete conversion was achieved (Figure 1). This motivated the synthesis of gold containing catalyst using a support consisting of 50 wt.% γ -Al₂O₃ and boehmite (aluminum oxyhydroxide γ -AlOOH, shortly denoted as Al₂O₃-b), namely Au/Co-Ce/Al catalyst (see *Sample preparation*) which exhibited a superior catalytic activity. Target oxidation to CO₂ and H₂O was reached by 95% HCHO conversion at room temperature and full conversion at 40 °C. The most active sample developed in this study was compared with the activity of reference catalysts for HCHO conversion reported in the literature (Table S1 in Supporting Material). The comparison clearly demonstrated that our best catalyst outperformed the activity exhibited by previously reported Co₃O₄-CeO₂-supported Au-based catalysts. The differences are especially relevant if catalyst composition and inlet HCHO concentration are considered. Additionally, we used simple mechanochemical mixing for the preparation of carriers in contrast to the quite complicated and time-consuming precursor thermal decomposition-assisted colloidal crystal templating method employed by Liu et al. [25]. This approximated comparison confirms the promising performance and economic profitability of the developed gold deposition on the multicomponent Co₃O₄-CeO₂-Al₂O₃ support.

Analysis of cost effectiveness in case of possible commercial application reasonably provokes the important question about stability and durability of supported gold catalysts. Therefore, HCHO oxidation activity at 40 °C was evaluated for all gold-based samples within a 100 h test duration. Stability tests demonstrated the same HCHO conversion into CO₂.

In-depth analysis of the role of support composition in HCHO oxidation over the studied gold catalysts was based on the results of sample characterization.

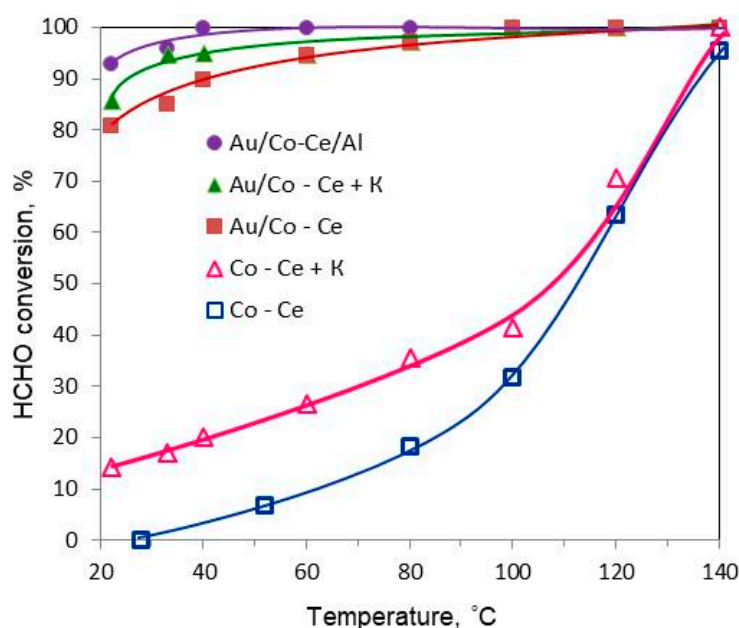


Figure 1. Temperature dependence of HCHO conversion over the studied samples.

2.2. Sample Characterization

Specific surface area (SSA), total pore volume (V_{pore}), and average pore diameter (D_{pore}) of the studied samples are listed in Table 1. Potassium addition led to a lower SSA value of Co-Ce+K as compared to that of Co-Ce mixed oxide. Haneda et al. [30] obtained an increased Co_3O_4 surface area by the addition of alkali metals up to a certain M/Co ratio followed by a decreasing trend. Ma et al. registered a 25% decrease in Na/ CeO_2 (2 wt.% Na) SSA with respect to CeO_2 and suggested the filling of some ceria pore structures caused by added sodium [31]. Accordingly, the worse Co-Ce+K textural properties, as observed in the present case, could be explained through Co–Ce pore blocking by K species. Differently, gold deposition played a positive role as acquired values of SSA, V_{pore} , and D_{pore} of Au/Co-Ce and especially of K-modified Au/Co-Ce+K are quite similar to those of the initial K-free Co-Ce sample. These data are in agreement with Reina et al. [32], who observed increased surface area and pore volume of Au/ CeO_2 -ZnO/ Al_2O_3 catalysts relative to bare supports and consistent with Gabrovská et al., who proposed new mesopore formation by gold in NiAl LDH (layered double hydroxide) [33]. The Au/Co-Ce/Al catalyst exhibited the best textural properties due to the Al_2O_3 -b contribution to the support composition.

Table 1. Specific surface area (SSA), pore volume (V_{pore}), and average pore diameter (D_{pore}) of the studied samples; average size and lattice parameter of Co_3O_4 ($D_{\text{Co}_3\text{O}_4}$ and $a_{\text{Co}_3\text{O}_4}$) and ceria (D_{CeO_2} and a_{CeO_2}) evaluated by XRD.

Sample	SSA ($\text{m}^2 \text{g}^{-1}$)	V_{pore} ($\text{cm}^3 \text{g}^{-1}$)	D_{pore} (nm)	$D_{\text{Co}_3\text{O}_4}$ (nm)	$a_{\text{Co}_3\text{O}_4}$ (Å)	D_{CeO_2} (nm)	a_{CeO_2} (Å)
Co-Ce	72	0.24	13.3	20.20	8.074 (5)	8.16	5.410 (7)
Co-Ce+K	43	0.19	17.9	18.95	8.078 (1)	7.13	5.422 (1)
Au/Co-Ce	68	0.25	14.9	19.46	8.081 (1)	6.96	5.418 (1)
Au/Co-Ce+K	65	0.24	13.1	20.32	8.080 (1)	6.96	5.418 (1)
Al_2O_3 -b	219	0.40	7.4				
Au/Co-Ce/Al	158	0.34	8.5	17.66	8.081 (2)	7.64	5.420 (2)

Figures in parentheses give the error of the last listed decimal digit.

Powder X-ray diffraction (XRD) patterns of the studied Co-Ce mixed oxides and gold catalysts are illustrated in Figure 2. The coexistence of the Co_3O_4 phase with the cubic spinel-type structure and cubic fluorite type CeO_2 phase is clearly seen. In all cases, CoO was not registered. High gold dispersion in Au containing catalysts has to be assumed since even the most intense typical reflection of metallic Au (111) at $2\theta = 38.2^\circ$ was not detectable. Reflections of the potassium phase for K-modified samples were also missing. No M-composite oxides were detected for doped Co_3O_4 via impregnation ($M = \text{K}, \text{Rb},$ and Cs with $M/\text{Co} = 0.035$) as reported by Haneda et al. [30]. The potassium compound was not registered by XRD due to the low concentration and/or high dispersion of K-containing species. However, potassium presence in the catalyst pores has to be considered based on the above-commented textural properties.

Co_3O_4 and CeO_2 average crystallite size ($D_{\text{Co}_3\text{O}_4}$ and D_{CeO_2}) as well as cobalt oxide and ceria lattice constants ($a_{\text{Co}_3\text{O}_4}$ and a_{CeO_2}) were evaluated based on XRD analysis and are displayed in Table 1. There is no significant difference in the ceria average particle size (6.96–8.16 nm). The average particle size of Co_3O_4 is also quite similar, and the lowest value of 17.66 nm was calculated for the Au/Co-Ce/Al catalyst. A slight expansion of Co_3O_4 and CeO_2 lattice in K- and Au-containing samples is seen compared with the initial Co-Ce sample. This effect caused by potassium could be explained by the possible incorporation of K^+ ions having a radius of 1.38 Å as compared to Ce^{4+} , Co^{2+} , and Co^{3+} radii of 1.01, 0.79, and 0.64 Å, respectively. The Co-Ce mixed oxide preparation by grinding procedure determined the surface structural disorder characterized by Co lattice contraction as the magnified patterns in 2θ range of $36\text{--}38^\circ$ showed a shift of Co_3O_4 (311) plane position toward higher degree values [29,34]. The slight expansion of the Co_3O_4 and CeO_2 lattice could be related to decreased lattice defectiveness determined by gold deposition. It is known that defects, such as oxygen vacancies, are preferential sites for Au nucleation at the surface of Co_3O_4 [35] (and references therein) and ceria [36]. However, lattice parameters were not strongly affected by potassium and/or gold addition since the undergone structural changes are located at the surface and near-surface region.

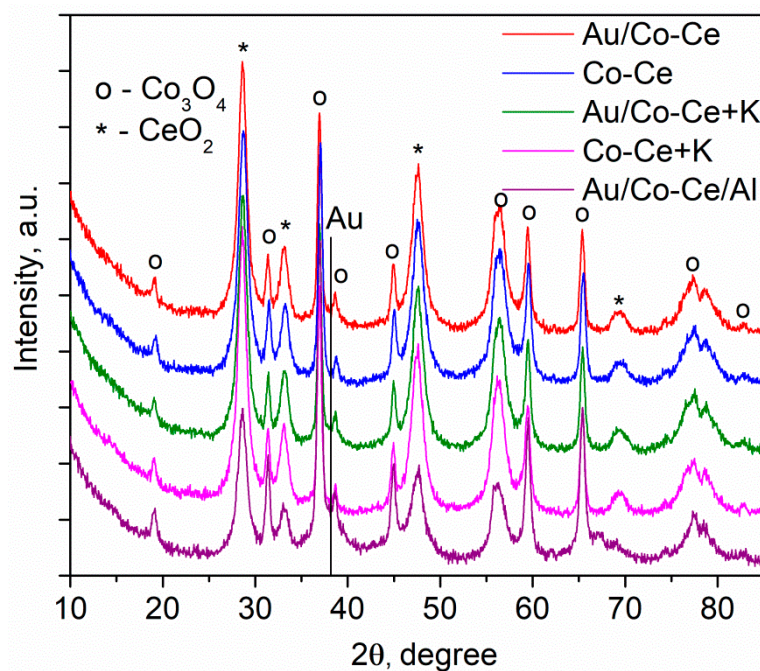


Figure 2. XRD patterns of the studied samples.

In order to gain more insight into existing phases at the surface of gold catalysts, a careful analysis of transmission electron microscopy (TEM) and selected high-resolution transmission electron microscopy (HRTEM) images was carried out. Figure 3 shows a

TEM image at magnification of $40,000\times$ (a) and HRTEM micrograph (b) of Au/Co-Ce sample. The measured interplanar distances of the exposed crystal planes correspond to gold (cubic, $a = 4.07825 \text{ \AA}$, COD # 96-900-8464) and cerium oxide phase $\text{Ce}_{11}\text{O}_{20}$ (triclinic, $a = 6.75700 \text{ \AA}$, $b = 10.26000 \text{ \AA}$, $c = 6.73200 \text{ \AA}$, $\alpha = 90.040^\circ$, $\beta = 99.800^\circ$, $\gamma = 96.220^\circ$, COD # 96-152-1461). Non-stoichiometric $\text{Ce}_{11}\text{O}_{20}$ could be interpreted as an intermediate phase of $\text{CeO}_2 \rightarrow \text{Ce}_2\text{O}_3$ reduction. Its crystal structure could be related to the fluorite structure of CeO_2 from which it is derived by vacancy formation during the reduction [37]. In some images (not shown in a figure), the Co_3O_4 phase (cubic, $a = 8.17730 \text{ \AA}$, COD # 96-900-5894) was distinguished but no gold particles in close vicinity were visible. This observation of low gold loading on cobalt oxide phase agrees with the suggestion of Liu et al. [25] and Wang et al. [38] about the preferential location of gold particles on ceria with respect to Co_3O_4 over the studied Au/ CeO_2 - Co_3O_4 catalysts.

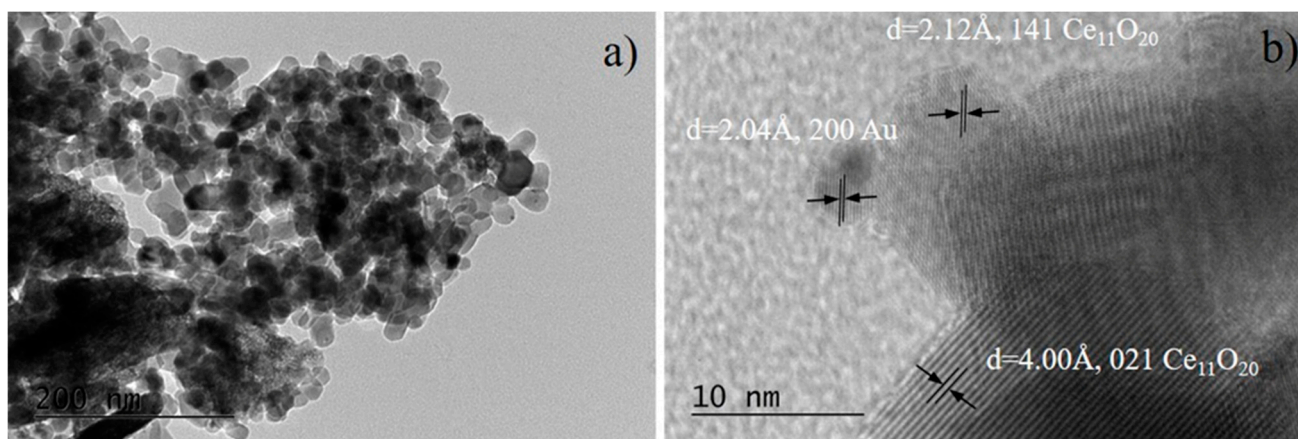


Figure 3. TEM image at magnification $40,000\times$ (a) and HRTEM image at magnification $600,000\times$ (b) for Au/Co-Ce sample.

TEM (Figure 4a,c) and HRTEM images (Figure 4b,d) of Au/Co-Ce/Al sample provided information that small gold particles were deposited also on a free alumina surface. The measured interplanar distances in Figure 4b correspond to gold on the ceria phase as shown above for the Au/Co-Ce sample, but also nanoparticles of gold on γ - AlOOH (orthorhombic, $a = 12.22700 \text{ \AA}$, $b = 3.70000 \text{ \AA}$, $c = 2.86600 \text{ \AA}$, COD # 96-900-9156) and γ - Al_2O_3 (triclinic, $a = 3.40090 \text{ \AA}$, $b = 2.78950 \text{ \AA}$, $c = 7.07620 \text{ \AA}$, $\alpha = 90.000^\circ$, $\beta = 90.000^\circ$, $\gamma = 90.000^\circ$, COD # 96-400-2419) can be clearly distinguished (Figure 4d). Available data do not allow a reliable statistical analysis to obtain size distribution histograms of gold particles. However, based on performed measurements and collected images, the average particle size seems to be in the range of 3–4 nm for gold particles deposited on both ceria and alumina (Figure 4b,d). The intimate interaction between gold and ceria is the well-known ability to bring stabilization of highly dispersed gold. Our own recent studies indicated quite large gold particles (44 nm) on γ -alumina using the deposition–precipitation method [39]. The present results are in accordance with Chen et al. [40], who gave evidence of highly stable nano-gold over γ - Al_2O_3 enriched with surface hydroxyl groups, which act as “ligands” upon binding gold species. In the case of Au/Co-Ce/Al catalyst, the hydroxylated surface of Al_2O_3 -b allowed attaching highly dispersed gold particles by the widely used deposition–precipitation method. The results agree with XRD observation of undetectable Au species for all studied gold catalysts.

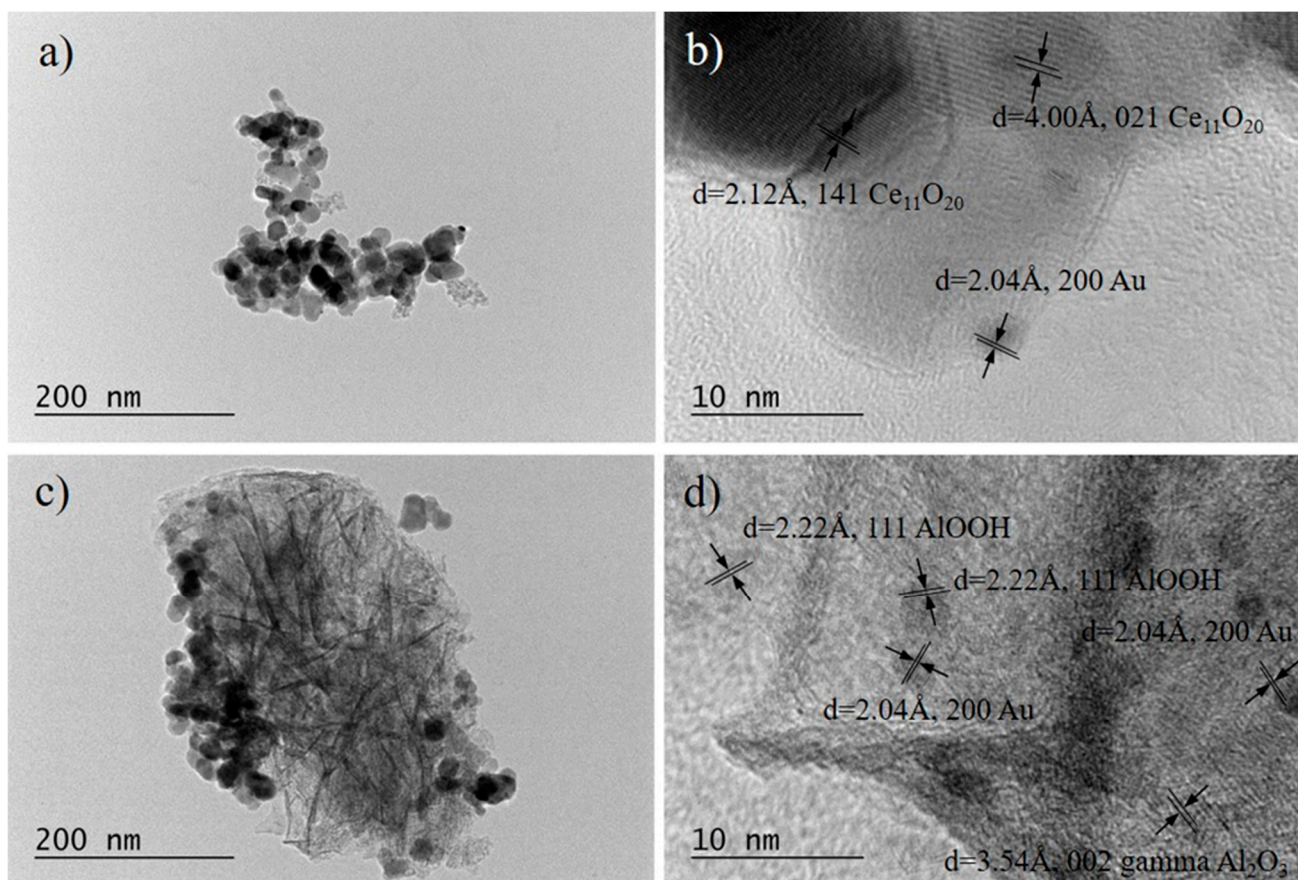


Figure 4. TEM images at magnification $40,000\times$ (a,c) and the corresponding HRTEM images at magnification $600,000\times$ (b,d) for two different zones of Au/Co-Ce/Al sample.

Catalyst reducibility was evaluated by H_2 -TPR (temperature-programmed reduction) measurements from room temperature to $800\text{ }^\circ\text{C}$ (Figure 5a). TPR profiles of Co-Ce and Co-Ce+K samples are similar to those usually obtained with bare Co_3O_4 for characteristic peaks of stepwise $Co^{3+} \rightarrow Co^{2+}$ and $Co^{2+} \rightarrow Co^0$ reduction [41]. Ceria reduction is characterized by bulk reduction at temperatures around $800\text{ }^\circ\text{C}$ through hardly visible low intense peaks and reduction of CeO_2 surface layers without affecting the fluorite structure around $500\text{ }^\circ\text{C}$ [42]. For the case of Co_3O_4 - CeO_2 mixed oxides, the latter process occurs in the temperature range of Co_3O_4 reduction due to the influence of the close contact with the cobalt phase [43].

Modification by potassium did not lead to the expected enhanced Co_3O_4 reducibility as reported by Bai et al. [17] and Fan et al. [18]. Despite higher T_{max} of $Co^{3+} \rightarrow Co^{2+}$ reduction after Co_3O_4 doping with KNO_3 and KCl , a lower T_{max} , i.e., better reducibility, was established using K_2CO_3 [19]. In the present study, T_{max} of both TPR peaks for K-containing mixed oxide was shifted by about $25\text{ }^\circ\text{C}$ toward higher temperatures in accordance with the reported effect of alkali metals on suppressed oxygen mobility by Tang et al. [20].

In the presence of small gold particles as proved by HRTEM, one complex TPR peak was recorded with the Au/Co-Ce catalyst. A very similar TPR peak in terms of shape and position was recorded for the Au/Co-Ce+K sample as well. Such a reduction behavior of Au/ CeO_2 - Co_3O_4 catalysts was already observed and explained by the predominant effect of gold upon $Co^{2+} \rightarrow Co^0$ reduction, leading to a second TPR peak shifted toward lower temperatures and thus overlapping with the former one [25,38]. Two peak characteristics of Co_3O_4 reduction are visible in the TPR profile of Au/Co-Ce/Al catalyst. The effect of gold for facilitated reduction is significant, and both TPR peaks are located at lower temperatures by about $50\text{ }^\circ\text{C}$ as compared to Co-Ce mixed oxide (Figure 5a).

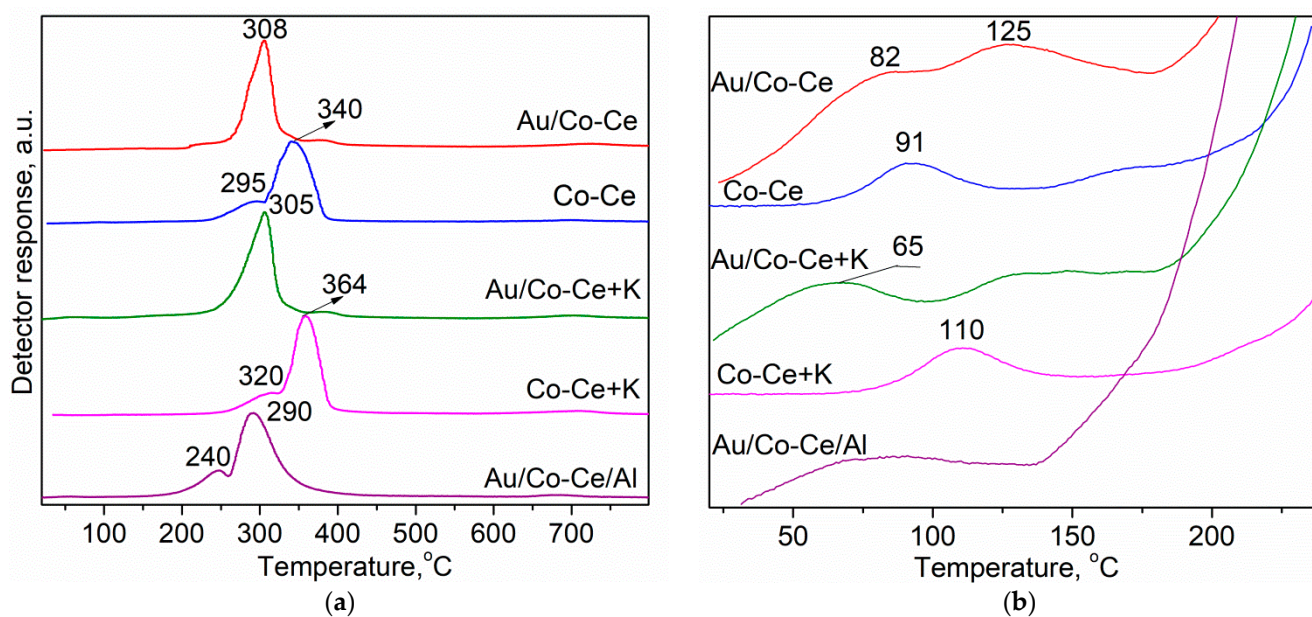


Figure 5. TPR profiles of the studied samples: (a) in the temperature range up to 800 °C; (b) in the temperature range up to 250 °C.

The aforementioned reduction behavior is related to bulk reducibility, which is informative about oxygen mobility dependency on sample structural features. However, like the present case of interaction between Co and Ce phases caused by mechanochemical preparation, the state of defective surface becomes of crucial importance by considering the Langmuir–Hinshelwood mechanism as more favorable via O₂ and HCHO coadsorption [44]. Accordingly, in a recent review on noble metal-based catalysts for formaldehyde oxidation, Guo et al. [2] (and references therein) commented that the reducibility of support materials is not a key factor that directly affects catalytic activity. The HCHO oxidation reaction is of interest at low temperatures, thus insuring reduction of operating costs. Regarding this item supplemental TPR measurements focused on hydrogen consumption up to 250 °C were performed. Figure 5b displays patterns which do not indicate a higher amount of surface-adsorbed oxygen species on Co-Ce+K as compared to the Co-Ce sample, i.e., there is no clear positive effect due to presence of potassium. A relatively higher hydrogen consumption is seen for the Au/Co-Ce catalyst. In this case, it should be related both to the surface oxygen species and ceria surface layer reduction. The role of nano-gold particles for considerable lowering the temperature of ceria surface layer reduction has been well known for already two decades [45]. The less intense peaks of Au/Co-Ce+K could be explained by assuming hardly affected ceria surface layers by gold reduction in the presence of potassium. Ma et al. [31] established inhibiting role of sodium species in the reduction of Na/CeO₂ and Ag-Na/CeO₂ catalysts. Interestingly, the reduction of Au/Co-Ce/Al catalyst commenced at the lowest possible temperature below 150 °C. Ceria surface layer reduction enhanced by gold and substantially facilitated Co³⁺ → Co²⁺ reduction have to be considered.

Surface chemical properties were compared based on X-ray photoelectron spectroscopy (XPS) measurements used for the estimation of element percentage composition and oxidation state. Ce 3d, Co 2p, and O 1s XP spectra of the studied samples are displayed in Figures 6 and 7. Au 4f spectra of gold catalysts, K 2p spectrum registered only for Co-Ce+K sample, and Al 2p signal related to the presence of Al₂O₃ and boehmite in Au/Co-Ce/Al catalyst are not illustrated. The results of the XPS analysis are shown in Tables 2 and 3.

Table 2. XPS quantitative analysis.

Sample	Au (at.%)	Ce (at.%)	Co (at.%)	Ce/Co 0.10 ¹	O (at.%)	K (at.%)	Al (at.%)
Co-Ce	-	13.1	19.0	0.69	67.9	-	-
Co-Ce+K	-	11.4	16.6	0.69	68.5	3.5	-
Au/Co-Ce	0.4	15.1	18.2	0.83	66.3	-	-
Au/Co-Ce+K	0.3	16.3	19.3	0.84	64.1	-	-
Au/Co-Ce/Al	0.4	2.9	16.1	0.19	64.1	-	16.4

¹ Nominal value.

Figure 6 depicts the registered Ce 3d spectra. The curves were fitted with ten peaks corresponding to five pairs of spin-orbit doublets (U and V refer to 3d_{3/2} and 3d_{5/2} spin-orbit components, respectively). One couple (U and V peaks) corresponds to one of two possible electron configurations of the final state of Ce³⁺ species. Binding energy (BE) of Ce 3d_{5/2} V component and calculated Ce³⁺/Ce_t atomic ratios, where total amount Ce_t = Ce⁴⁺ + Ce³⁺, are given in Table 3. Ce³⁺/Ce_t ratio values between 0.26 and 0.40 indicate a defective surface ceria structure, in particular a high amount of oxygen vacancies, because Ce³⁺/Ce_t values typical of bulk ceria are within 0.06–0.11 [46] (and references therein). Enhanced Ce³⁺ formation in the presence of closely spaced Co₃O₄ species was considered favorable for the oxidation of hydrocarbons [47] (and reference therein). Gold presence caused the highest Ce³⁺ surface amount in Au/Co-Ce and Au/Co-Ce/Al catalysts and in agreement, the HRTEM measurements of these gold catalysts evidenced Ce₁₁O₂₀ species at the surface. It could be assumed that potassium hindered this process in accordance with lower Ce³⁺ concentration detected in the Au/Co-Ce+K sample (Table 3).

Co 2p spectra (Figure 7a) are characterized by 2p_{3/2} and 2p_{1/2} spin-orbit components with intensity ratio of 2:1. Observed spin-orbit splitting around 15.2 eV suggests mixed valence Co₃O₄ [26]. Cobalt oxidation states were distinguished after the fitting of each 2p component by two corresponding curves. For all studied samples, deconvolution of the 2p_{3/2} component consisted of a more intense peak at BE 779.9 ± 0.2 eV assigned to Co³⁺ and another weaker peak at 781.8 ± 0.1 eV typical of Co²⁺ ions (Table 3).

Analogous to data reported in the literature, the Co 2p components characteristic of Co²⁺ were accompanied by shakeup features about 6 eV at the high-energy side from the main peaks [48]. Table 3 presents Co³⁺/Co_t (total amount Co_t = Co³⁺ + Co²⁺) values which are higher than nominal 0.67 for stoichiometric Co₃O₄. In agreement with the reported data about Co₃O₄-CeO₂ mixed oxides, close interaction with ceria could maintain cobalt in a high oxidation state as Co³⁺ [47,49–51]. A higher Co³⁺/Co_t ratio for Co-Ce+K as compared to Co-Ce was established because the lattice distortion and interaction between potassium and Co₃O₄ could promote the generation of more active Co³⁺ at the surface [17,52]. No difference in Co³⁺/Co_t ratio was visible for Au/Co-Ce and Au/Co-Ce+K catalysts. In the latter case, K 2p signal was not detected, suggesting the covering of potassium by gold or K migration inside the sample during the final calcination procedure. A lack of substantial difference in the TPR profiles of these samples (Figure 5a) could also be explained by the missing influence of potassium after Au deposition.

Calculated Ce/Co ratios (Table 2) for Co-Ce, Co-Ce+K, and especially for the corresponding gold catalysts, are much higher than nominal values. A similar significant enrichment of Ce-Co mixed oxide surface by ceria was also reported [26,51]. Close interaction between Co phase covered by ceria and gold deposited mainly on ceria as already shown by the HRTEM data and in agreement with the literature reports could be the reason for the TPR behavior of Au/Co-Ce and Au/Co-Ce+K catalysts. Prevailing Co²⁺ reduction enhancement was supposed based on the above-commented literature data resulting in only one complex TPR peak (Figure 5a), unlike the two peaks related to a two-step Co₃O₄ reduction. However, such a close interaction was not achieved at the surface of Au/Co-Ce/Al. The Ce/Co ratio consistent with the nominal value indicated that ceria surface

segregation did not occur, and gold on cobalt oxide substantially enhanced both Co^{3+} and Co^{2+} reduction typically characterized by the registration of two TPR peaks.

Table 3. XPS binding energies and atomic ratios.

Sample	Au 4f _{7/2} (eV)	Ce 3d _{5/2} (eV)	Ce ³⁺ /Ce _t	Co 2p _{3/2} (eV)	Co ³⁺ /Co _t	O 1s (eV)	O _s /O _l	K 2p _{3/2} (eV)	Al 2p (eV)
Co-Ce	-	882.3	0.33	779.8 (73) 781.7 (27)	0.73	529.9 (77) 531.9 (21) 533.4 (02)	0.27	-	-
Co-Ce+K	-	882.2	0.26	779.7 (84) 781.9 (16)	0.84	529.7 (79) 531.8 (21)	0.26	293.2	-
Au/Co-Ce	84.6	882.6	0.40	780.1 (74) 781.9 (26)	0.74	530.2 (62) 532.2 (28) 533.5 (10)	0.45	-	-
Au/Co-Ce+K	84.5	882.4	0.29	779.9 (75) 781.8 (25)	-	529.9 (67) 532.0 (25) 533.5 (08)	0.37	n.d.	-
Au/Co-Ce/Al	84.3	882.3	0.40	780.0 (78) 781.7 (22)	0.78	530.2 (60) 532.1 (35) 533.0 (05)	0.58	-	74.6

Values in parentheses are the relative areas of the corresponding peak. O_s/O_l is calculated from the ratio of the low energy O 1s component (at about 530 eV) over the intermediate energy O 1s component (around 532 eV). n.d.—not detected.

Experimental and fitted O 1s spectra are shown in Figure 7b. Three components with BEs given in Table 3 can be distinguished. The most intense one at about 530 eV is assigned to lattice oxygen (O_l), and a component with intermediate BE around 532 eV (O_s) is ascribed to surface chemisorbed species containing oxygen as O²⁻, O⁻, O₂²⁻ [49,53,54]. Surface hydroxyl groups and/or defect oxide oxygen can be distinguished [51,55,56], and a small component at a higher BE is assigned to oxygen-carbon bonds arising from some impurity [54].

Very similar O_s/O_l ratios for Co-Ce and Co-Ce+K samples (Table 3) do not support the expectation of larger amounts of surface hydroxyl groups and oxygen species (as also shown by TPR) due to added potassium. A higher availability of OH groups and oxygenated species occurred at the surface of Au/Co-Ce catalyst; however, yet again unexpected, potassium presence caused a lower O_s/O_l value. Obtained results revealed the most abundant oxygen containing species at the surface of Au/Co-Ce/Al that is reasonably explained by the contribution of the boehmite OH groups.

The Au 4f region showed two spin-orbit components (4f_{7/2} and 4f_{5/2}), and the obtained Au 4f_{7/2} BEs are given in Table 3. According to the literature data for supported gold catalysts, the Au 4f_{7/2} photoelectron peak located at 84.1–84.2 eV is usually assigned to metallic gold. Depending on the support, the BE of 84.4 eV was also related to Au⁰ [57] (and references therein). BE values in Table 3 can be interpreted as informative for the presence of partially oxidized Au^{δ+} particles.

The relationship between gold oxidation state and activity for HCHO oxidation is still under debate. A positive role of cationic gold was proposed mainly with respect to Au/CeO₂ catalysts [58–61]. Some discrepancy existed for the role of the gold oxidation state when Au/Co₃O₄-CeO₂ catalysts were studied. Liu et al. [25] explained 3DOM Au/Co₃O₄-CeO₂ catalyst deactivation by weaker carrier interaction due to solely registered metallic gold in the spent samples. However, in some studies, Au⁰ was considered highly effective for HCHO oxidation. Ma et al. [5] established mainly metallic gold state in 2D Au/Co₃O₄-CeO₂ catalysts.

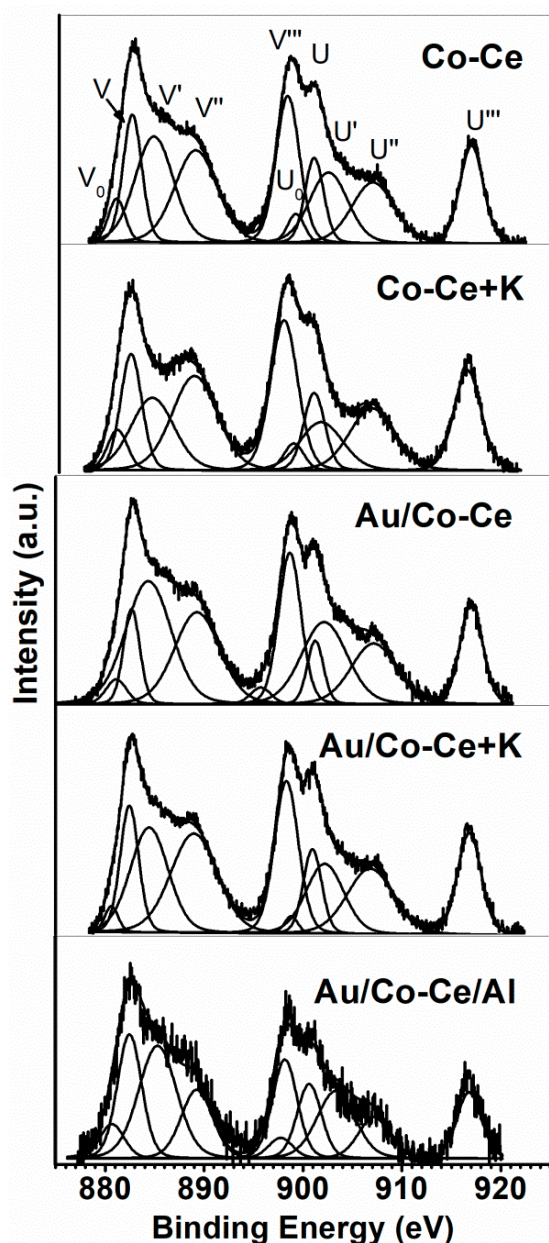


Figure 6. Ce 3d XP spectra of the studied samples.

Gold oxidation state and especially gold particle size are key factors for HCHO oxidation activity. On the other hand, carrier composition, structure, and properties are also of crucial importance. Recent comparison between mechanochemically prepared mixed oxides containing 80, 70, or 60 wt.% Co_3O_4 and respective 20, 30, or 40 wt.% CeO_2 showed surface structural defects caused by the mechanochemical treatment [29]. The presence of structural disorder was considered favorable for larger Co–O bond length, making easier oxygen vacancy formation, thus leading to easier oxygen extraction from the surface of Co_3O_4 [62]. The highest surface defectiveness caused by close interaction between Co_3O_4 and CeO_2 phases was observed for the optimal composition of 70 wt.% Co_3O_4 and 30 wt.% CeO_2 and evidenced the highest amount of Co^{3+} , Ce^{3+} and adsorbed oxygen species [29]. This determined the chosen composition of the Co-Ce support for the present investigation.

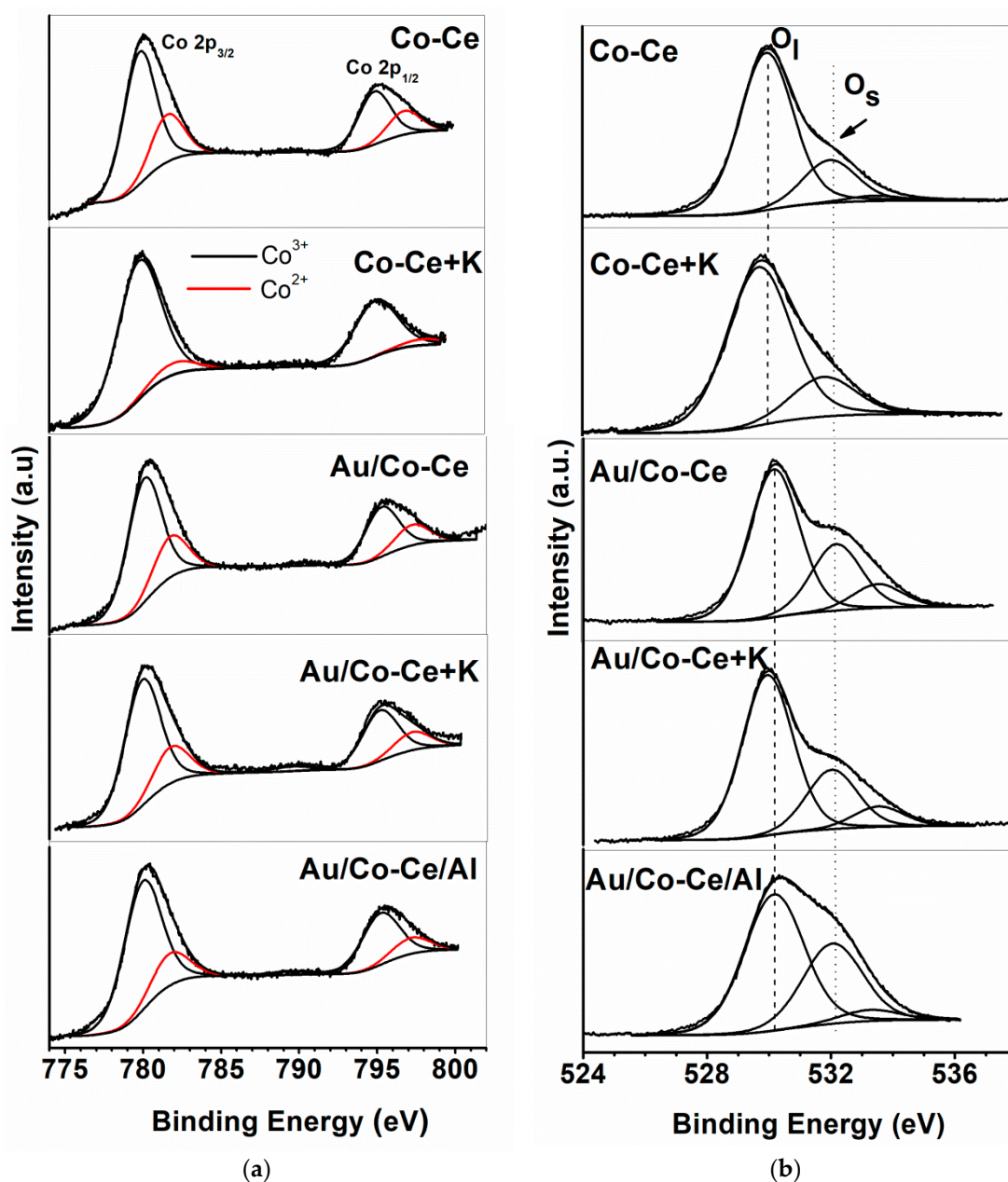


Figure 7. Co 2p XP spectra (a), and O 1s XP spectra (b) of the studied samples.

On studying $\text{Co}_3\text{O}_4\text{-CeO}_2$ containing catalysts, Ma et al. [5] suggested a reaction mechanism involving HCHO adsorption on Co_3O_4 with Co^{3+} as the main active entities and the formation of CHO species followed by oxidation of the latter by surface active oxygen to formate HCOO^- species and further transformed to CO_2 . Bai and Li proposed a pathway over $\text{K-Ag/Co}_3\text{O}_4$ catalysts, including the direct participation of generated OH groups by added alkali metal in the HCOO^- conversion to $\text{CO}_2 + \text{H}_2\text{O}$. The authors commented also the role of hydroxyl groups to facilitate the migration of O^{2-} species [17]. To clarify the reaction mechanism in the presence of surface defects, Deng et al. [44] used a combination between DFT calculations and microkinetic modeling of HCHO oxidation over Co_3O_4 . The suggestion involved surface oxygen species participating in the first C–H bond cleavage by the formation of formate species followed by a second C–H bond cleavage to transform the formate group to CO_2 through oxygen adsorption on a neighbor oxygen vacancy or active oxygen diffusion from other sites. The authors disclosed the effect of OH groups on active oxygen diffusion. They also presented another role of isolated OH species

to decrease dissociation barrier of the two C–H bonds of HCHO. In the present case, the improved performance of the Co-Ce+K sample especially in the lower temperature range is visible (Figure 1). However, O_s/O_l ratios obtained by XPS (Table 3) did not indicate a higher amount of surface oxygen containing species, in particular, higher OH group coverage. A lack of intense hydrogen consumption during TPR in the low temperature range (Figure 5b) gave no reason to assume more oxygen species at the Co-Ce+K surface as compared to Co-Ce. An explanation of higher HCHO oxidation activity of Co-Ce+K than that of Co-Ce could be the highest Co^{3+}/Co_t ratio (Table 3). The structure–catalytic activity relationship has been often associated with concentration of the surface Co^{3+} species responsible for HCHO activation [3] (and references therein). Sun et al. showed the role of increased Co^{3+} amount to promote the abundance of anion defects in particular oxygen vacancies [63]. Bai and Li also reported [17] that the Co^{3+} species may increase the number of oxygen vacancies, which directly participate in oxygen adsorption, activation, and migration, thus enhancing the catalytic activity of Co_3O_4 . Similar Co^{3+}/Co_t ratio values were calculated for both Au/Co-Ce and Au/Co-Ce+K. The latter catalyst demonstrated only a slightly better performance (Figure 1). Modification by potassium caused less enhancement of HCHO oxidation activity as expected by the authors. Gold deposition on Co-Ce support led to a remarkable improvement of the catalytic performance related to high amount of O_s species established by XPS as well as high amount of surface Co^{3+} and Ce^{3+} species that suggested also an abundance of defects, such as oxygen vacancies. It was reported that charged oxygen species (O^{2-} , O_2^{2-} , O_4^{2-}) can easily be formed by localized electrons at surface oxygen vacancies [9] (and references therein). Besides the indisputable role of oxygen vacancies for active oxygen species generation and migration [44], some authors commented a possible positive role of oxygen vacancies as basic Lewis sites because both formaldehyde and the intermediate formate species react as a Lewis acid [64]. A reaction mechanism, including the synergistic effect, among gold nanoparticles, CeO_2 , and Co_3O_4 was proposed to explain enhanced catalytic activity in HCHO oxidation [5,25,27]. Au/Co-Ce and Au/Co-Ce+K catalysts (Figure 1) were highly active around room temperature. However, target complete HCHO conversion to CO_2 and H_2O was not reached. This observation initiated the mechanochemical preparation of new support for gold deposition using $\gamma-Al_2O_3$ containing boehmite on purpose. The goal was to achieve a dual advantage by including a component of high surface area and hydroxyl coverage (unachieved by K modification) and reduction in catalyst price by lowering cobalt and cerium oxides amount. The Au/Co-Ce/Al gold-containing catalyst exhibited a superior catalytic activity by 100% conversion to CO_2 and H_2O at 40 °C. In addition to the high-performing Au/Co-Ce phase, the contribution of small gold particles on hydroxylated alumina has to be considered. This supposition is in accordance with the study of Chen and coauthors [40,65], showing $\gamma-Al_2O_3$ -supported gold as a very active catalyst for room temperature HCHO oxidation. The presence of gold of small dimensions on a bare alumina surface of Au/Co-Ce/Al was evidenced by HRTEM analysis and further supported by XRD results of undetectable gold. Hydroxyl groups capable of participating in C–H bond cleavage were commented above. The results of XPS analysis showed the highest O_s/O_l ratio for Au/Co-Ce/Al catalyst and was reasonably explained by the contribution of boehmite OH groups. Furthermore, high Ce^{3+}/Ce_t ($Ce_{11}O_{20}$ phase at the surface) and Co^{3+}/Co_t ratios were calculated. A TPR measurement of Au/Co-Ce/Al focused on the low temperature range revealed the lowest temperature of the reduction start-up. In this case, the effect of gold to enhance the reduction of both ceria surface layers and $Co^{3+} \rightarrow Co^{2+}$ was the most pronounced, bearing in mind the weakly bonded and readily interacting oxygen in the near-surface region of the catalyst. The results revealed gold contribution to both the highly hydroxylated Al_2O_3 -b and defective Co-Ce mixed oxide surface for excellent catalytic activity in HCHO oxidation. Future research efforts will be focused on the optimization of the composition, aiming to improve economic profitability by lowering the content of the Co-Ce mixed oxide.

3. Materials and Methods

3.1. Catalyst Preparation

Co₃O₄-CeO₂ mixed oxide was synthesized by cerium hydroxide and cobalt hydroxycarbonate precursors using calculated amounts to compose 70 wt.% Co₃O₄ and 30 wt.% CeO₂. The mixture was subjected to grinding in an electric mortar (Mortar Grinder RM 200, Retsch, Haan, Germany) for 1 min. The detailed procedure is described in our previous study [29]. Calcination in air at 400 °C for 2 h yielded the Co₃O₄-CeO₂ mixed oxide, which is denoted as Co-Ce. It was modified by wet impregnation with 3 wt.% K₂CO₃, the optimal concentration being proposed in Ref. [19]. This was followed by calcination at 400 °C for 2 h. Notation of the obtained sample is Co-Ce+K.

Gold (3 wt.%) was loaded on the Co-Ce and Co-Ce+K supports suspended in water by the deposition–precipitation method via interaction between HAuCl₄·3H₂O and K₂CO₃ under vigorous stirring at constant pH = 7.0 and temperature of 60 °C. After ageing for 1 h at the same temperature, filtering, and abundant washing until the removal of chlorine ions, the precipitates were dried at 80 °C under vacuum and calcined in air at 400 °C for 2 h. The gold catalysts were named Au/Co-Ce and Au/Co-Ce+K. Samples of gold on CeO₂ and Co₃O₄, denoted as Au/Ce and Au/Co, respectively, were prepared for comparison. The initial salts used for catalyst preparation were of “analytical grade”.

Additionally, γ -Al₂O₃ containing boehmite (Al₂O₃-b) was used to prepare a support with high hydroxyl coverage. XRD and combined DTA/TG analysis for determination of boehmite amount (33.3%) are presented in the Supporting Material (Figures S2 and S3). The support consisted of 50 wt.% Al₂O₃-b as well as 35 wt.% Co₃O₄ and 15 wt.% CeO₂ in order to keep the chosen Co₃O₄/CeO₂ ratio. It was prepared by grinding preset amounts of Al₂O₃-b, cerium hydroxide, and cobalt hydroxycarbonate in the mortar for 1 min followed by calcination in air at 400 °C within 2 h. Gold (3 wt.%) was loaded by the deposition–precipitation method using the above-described procedure. The synthesized gold catalyst is denoted as Au/Co-Ce/Al.

3.2. Catalytic Activity Measurements

Catalytic tests in the reaction of HCHO oxidation were performed at atmospheric pressure by continuous flow equipment with a four-channel isothermal stainless-steel reactor, allowing simultaneous examination of four catalysts under the same conditions. Sample loading was 0.5 mL (0.6–1.0 mm pellets). Gaseous formaldehyde of 120 mL m⁻³ (120 ppm) generated by air flow passing through paraformaldehyde ($\geq 95.0\%$, Merck KGaA, Darmstadt, Germany) with a fixed temperature of 36 °C was introduced applying GHSV of 10,000 h⁻¹, and a subsequent experiment was provided using GHSV of 20,000 h⁻¹. Constant HCHO inlet concentration was controlled by means of the Faro 100 Spectrophotometer (Merck KGaA, Darmstadt, Germany). The catalytic measurements were carried out from 200 °C toward lower temperatures, having in mind that the opposite way of starting at room temperature might provoke HCHO polymerization. The CO₂ concentration at the reactor outlet was measured using an INTERSMAT IGC 112M gas chromatograph (Intersmat Instruments, Chelles les Coudreaux, France) with thermal conductivity detector (TCD) and Porapak-Q column. Analysis of possible products of incomplete HCHO oxidation as CO or hydrocarbon by-products was provided by HP 5890 Series II gas chromatograph (Agilent, Waldbronn, Germany) with Porapak-Q and MS-5A columns equipped with TCD and flame ionization detector (FID) detectors. Except for CO₂, no other carbon-containing products of HCHO oxidation were detected with all tested samples. HCHO conversion degree at each temperature was calculated by the following equation:

$$\text{HCHO conversion (\%)} = \frac{[\text{CO}_2]_{\text{outlet}}}{[\text{HCHO}]_{\text{inlet}}} \times 100,$$

where [HCHO]_{inlet} is the initial formaldehyde concentration in the gas flow and [CO₂]_{outlet} is the CO₂ concentration after reaction.

Long-term stability test was carried out at 40 °C within 100 h over all gold-based samples.

3.3. Catalyst Characterization

Specific surface area (SSA) of the samples was measured by analyzing N₂ adsorption isotherms at the temperature of liquid nitrogen. Calculated results were based on BET equation. Experiments were carried out in the 0.05–0.3 P/P0 standard pressure range, using NOVA 1200e Quantachrome Instrument (Boynton Beach, FL, USA). Prior to the measurements, the samples were degassed for 2 h under vacuum at 200 °C.

Powder X-ray diffraction measurements were carried out on a PANalytical Empyrean apparatus using a multichannel detector (Pixel 3D, PANalytical B.V., Almelo, the Netherlands), having Cu K_α 45 kV-40 mA radiation in the 2θ range 20–115° with a scan step of 0.01° for 20 s. The particle size of the crystalline phases and lattice parameters were evaluated by powder diffraction analysis software based on the Rietveld method (ReX) [66].

The morphology of the studied samples was evaluated by the Jeol JEM 2100 high-resolution transmission electron microscope (Jeol, Tokyo, Japan) at 200 kV accelerating voltage in conventional TEM mode. Diffraction methods for registration of sample phase composition were applied. Match software and Crystallographic Open Database (COD) was used for surface phase identification.

Two series of TPR experiments were performed. One of them involved TPR runs up to 800 °C by means of previously described apparatus [67] using a flow rate of 24 mL min⁻¹ of the reducing gas (10% H₂ in Ar) and temperature ramp rate of 15 °C min⁻¹. Following the criterion proposed by Monti and Baiker, the loaded sample amounts were 0.007 and 0.014 g for the Au/Co-Ce/Al catalyst [68]. The second one included TPR measurements up to 250 °C carried out by means of Chembet TPR/TPD apparatus (Quantachrome, Odelzhausen, Germany) using 5% H₂ in Ar with a flow rate of 80 mL min⁻¹ and a heating rate of 10 °C min⁻¹. The purpose of these TPR measurements was to distinguish and compare low intense hydrogen consumption in the latter temperature range. The loaded sample amounts were 0.03 and 0.06 g for the Au/Co-Ce/Al catalyst.

X-ray photoelectron spectroscopy analyses were carried out using a VG Microtech ESCA 3000 Multilab (VG Scientific, East Grinstead, Sussex, UK) spectrometer equipped with a dual Mg/Al anode following previously described procedure [69]. Constant charging of the samples was removed by referencing all the energies to the C 1 s binding energy set at 285.1 eV arising from the adventitious carbon. Peak analysis was performed by means of CasaXPS software. Atomic concentrations were calculated from peak intensity using sensitivity factors provided by the software. Binding energy values were quoted with a precision of ±0.15 eV and atomic percentage with a precision of ±10%.

4. Conclusions

The catalytic activity of gold catalysts in formaldehyde oxidation was discussed in line with the carrier composition and results of textural, XRD, HRTEM, TPR, and XPS characterization. Gold deposited on a mechanochemically synthesized Co₃O₄-CeO₂ mixed oxide carrier (70 and 30 wt.%, respectively) exhibited high HCHO oxidation activity. However, in the range around room temperature, the target complete HCHO conversion to CO₂ and H₂O was not reached. Expected significant improvement of the catalytic behavior of gold on Co-Ce mixed oxide modified by potassium was not achieved. Aiming to enhance the catalytic performance by increasing surface hydroxyl coverage as well as to reduce the catalyst cost, a new support material containing γ-Al₂O₃ and boehmite (named Al₂O₃-b, 50 wt.%) in addition to the Co-Ce mixed oxide with a selected ratio was prepared by mechanochemical mixing. The deposited gold on this carrier exhibited superior catalytic activity in agreement with established high Ce³⁺ and Co³⁺ surface amounts and the most abundant oxygen containing species with enhanced mobility. Results of 95% HCHO conversion to CO₂ and H₂O at room temperature and 100% conversion at 40 °C revealed an important contribution of gold supported on both highly hydroxylated Al₂O₃-b and defective Co-Ce mixed oxide surface. HCHO oxidation activity at 40 °C was evaluated

within a 100 h test duration. Stability tests demonstrated the same HCHO conversion into CO₂. Results of the study point to future optimization of support composition. Research efforts will be focused on the development of an efficient gold catalyst for room-temperature HCHO abatement with improved cost effectiveness by further lowering the amount of critical raw materials, such as cobalt and cerium oxides.

Supplementary Materials: The following supporting information can be downloaded at: <https://www.mdpi.com/article/10.3390/catal12070705/s1>, Figure S1. Comparison of HCHO conversion over Au/Ce, Au/Co, and Au/Co-Ce samples; Figure S2. XRD pattern of γ -Al₂O₃ used for preparation of Co₃O₄-CeO₂/Al₂O₃ support; Figure S3. DTA/TG analysis of γ -Al₂O₃; Table S1. HCHO conversion over the most active sample developed in this study compared with HCHO conversion over Co₃O₄-CeO₂-supported Au-based catalysts reported in the literature.

Author Contributions: Conceptualization, L.I. and T.T.; synthesis, T.T.; investigation: catalytic activity, D.D. and E.K.; XPS measurements and analysis, A.M.V.; TEM/HRTEM measurements and analysis, D.K.; XRD characterization, G.A.; TPR measurements, P.P. and R.S.; writing—original draft preparation, L.I.; writing—review and editing, A.M.V., D.K. and T.T. All authors have read and agreed to the published version of the manuscript.

Funding: APC was sponsored by MDPI.

Data Availability Statement: The data presented in this study are available in the article.

Acknowledgments: The paper is based upon work from COST Action INDIAIRPOLLNET CA17136. Financial support from Bulgarian Academy of Sciences through bilateral grant agreement between Bulgarian Academy of Sciences and Consiglio Nazionale delle Ricerche is gratefully acknowledged. Research equipment of Distributed Research Infrastructure INFRAMAT, part of Bulgarian National Roadmap for Research Infrastructures, supported by Bulgarian Ministry of Education and Science was used in this investigation.

Conflicts of Interest: The authors declare no conflict of interest.

References

1. Bai, B.; Qiao, Q.; Li, J.; Hao, J. Progress in research on catalysts for catalytic oxidation of formaldehyde. *Chin. J. Catal.* **2016**, *37*, 102–122. [[CrossRef](#)]
2. Guo, J.; Lin, C.; Jiang, C.; Zhang, P. Review on noble metal-based catalysts for formaldehyde oxidation at room temperature. *Appl. Surf. Sci.* **2019**, *475*, 237–255. [[CrossRef](#)]
3. Yusuf, C.; Snape, J.; He, H.; Xu, C.; Liu, M.; Zhao, G.Z.; Chen, B.; Tang, C.; Wang, J.; Behera, S.N. Advances on transition metal oxides catalysts for formaldehyde oxidation: A review. *Catal. Rev. Sci. Eng.* **2017**, *59*, 189–233. [[CrossRef](#)]
4. Li, R.; Huang, Y.; Zhu, D.; Ho, W.; Lee, S.; Cao, J. A Review of Co₃O₄-based catalysts for formaldehyde oxidation at low temperature: Effect parameters and reaction mechanism. *Aerosol Sci. Eng.* **2020**, *4*, 147–168. [[CrossRef](#)]
5. Ma, C.; Wang, D.; Xue, W.; Dou, B.; Wang, H.; Hao, Z. Investigation of formaldehyde oxidation over Co₃O₄-CeO₂ and Au/Co₃O₄-CeO₂ catalysts at room temperature: Effective removal and determination of reaction mechanism. *Environ. Sci. Technol.* **2011**, *45*, 3628–3634. [[CrossRef](#)]
6. Bai, B.; Arandiyani, H.; Li, J. Comparison of the performance for oxidation of formaldehyde on nano-Co₃O₄, 2D-Co₃O₄, and 3D-Co₃O₄ catalysts. *Appl. Catal. B Environ.* **2013**, *142–143*, 677–683. [[CrossRef](#)]
7. Wu, Y.; Ma, M.; Zhang, B.; Gao, Y.; Lu, W.; Guo, Y. Controlled synthesis of porous Co₃O₄ nanofibers by spiral electrospinning and their application for formaldehyde oxidation. *RSC Adv.* **2016**, *6*, 102127–102133. [[CrossRef](#)]
8. Chen, Y.; Guo, Y.; Hu, H.; Wang, S.; Ying, L.; Huang, Y. Achieving low temperature formaldehyde oxidation: A case study of NaBH₄ reduced cobalt oxide nanowires. *Inorg. Chem. Commun.* **2017**, *82*, 20–23. [[CrossRef](#)]
9. Wang, Z.; Wang, W.; Zhang, L.; Jiang, D. Surface oxygen vacancies on Co₃O₄ mediated catalytic formaldehyde oxidation at room temperature. *Catal. Sci. Technol.* **2016**, *6*, 3845–3853. [[CrossRef](#)]
10. Huang, F.; Chen, C.; Wang, F.; Wang, B.; Zhang, L.; Lu, S.; Li, K. Effect of calcination temperature on the catalytic oxidation of formaldehyde over Co₃O₄-CeO₂ catalysts. *Catal. Surv. Asia* **2017**, *21*, 143–149. [[CrossRef](#)]
11. Xie, S.; Dai, H.; Deng, J.; Liu, Y.; Yang, H.; Jiang, Y.; Tan, W.; Ao, A.; Guo, G. Au/3DOM Co₃O₄: Highly active nanocatalysts for the oxidation of carbon monoxide and toluene. *Nanoscale* **2013**, *5*, 11207–11219. [[CrossRef](#)] [[PubMed](#)]
12. Zhang, J.; Jin, Y.; Li, C.Y.; Shen, Y.N.; Han, L.; Hu, Z.X.; Di, X.W.; Liu, Z.L. Creation of three-dimensionally ordered macroporous Au/CeO₂ catalysts with controlled pore sizes and their enhanced catalytic performance for formaldehyde oxidation. *Appl. Catal. B Environ.* **2009**, *91*, 11–20. [[CrossRef](#)]

13. Huang, Y.; Fan, W.; Long, B.; Li, H.; Qiu, W.; Zhao, F.; Tong, Y.; Ji, H. Alkali-modified non-precious metal 3D-NiCo₂O₄ nanosheets for efficient formaldehyde oxidation at low temperature. *J. Mater. Chem. A* **2016**, *4*, 3648–3654. [[CrossRef](#)]
14. Xie, J.; Meng, M.; Tang, Y.; Yang, P.; Kang, C.; Zhou, Z.; Huang, S. Investigation of removal of HCHO by Zn modified Co₃O₄ catalyst at room temperature. *Res. Chem. Intermed.* **2019**, *45*, 3879–3893. [[CrossRef](#)]
15. Xie, J.; Meng, M.; Lin, Z.; Ding, H.; Chen, J.; Huang, S.; Zhou, Z. Exploring removal of formaldehyde at room temperature over Cr and Zn modified Co₃O₄ catalyst prepared by hydrothermal method. *Res. Chem. Intermed.* **2020**, *46*, 1789–1804. [[CrossRef](#)]
16. Baidya, T.; Murayama, T.; Bera, P.; Safonova, O.V.; Steiger, P.; Katiyar, N.K.; Biswas, K.; Haruta, M. Low-temperature CO oxidation over combustion made Fe- and Cr-doped Co₃O₄ catalysts: Role of dopant's nature toward achieving superior catalytic activity and stability. *J. Phys. Chem. C* **2017**, *121*, 15256–15265. [[CrossRef](#)]
17. Bai, B.; Li, J. Positive effects of K⁺ ions on three-dimensional mesoporous Ag/Co₃O₄ catalyst for HCHO oxidation. *ACS Catal.* **2014**, *4*, 2753–2762. [[CrossRef](#)]
18. Fan, Z.; Zhang, Z.; Fang, W.; Yao, X.; Zou, G.; Shangguan, W. Low-temperature catalytic oxidation of formaldehyde over Co₃O₄ catalysts prepared using various precipitants. *Chin. J. Catal.* **2016**, *37*, 947–954. [[CrossRef](#)]
19. Fan, Z.; Shi, J.; Zhang, Z.; Chen, M.; Shangguan, W. Promotion effect of potassium carbonate on catalytic activity of Co₃O₄ for formaldehyde removal. *J. Chem. Technol. Biotechnol.* **2018**, *93*, 3562–3568. [[CrossRef](#)]
20. Tang, W.; Weng, J.; Lu, X.; Wen, L.; Suburamian, A.; Nam, C.Y.; Gao, P.X. Alkali-metal poisoning effect of total CO and propane oxidation over Co₃O₄ nanocatalysts. *Appl. Catal. B Environ.* **2019**, *256*, 117859. [[CrossRef](#)]
21. Scirè, S.; Liotta, L.F. Supported gold catalysts for the total oxidation of volatile organic compounds. *Appl. Catal. B Environ.* **2012**, *125*, 222–246. [[CrossRef](#)]
22. Takei, T.; Akita, T.; Nakamura, I.; Fujitani, T.; Okumura, M.; Okazaki, K.; Huang, J.; Ishida, T.; Haruta, M. Heterogeneous catalysis by gold. In *Advances in Catalysis*; Gates, B.C., Jentoft, F.C., Eds.; Elsevier B.V.: Amsterdam, The Netherlands, 2012; Volume 55, pp. 1–124.
23. Gaálová, J.; Topka, P. Gold and ceria as catalysts for VOC abatement: A review. *Catalysts* **2021**, *11*, 789. [[CrossRef](#)]
24. Jing, M.; Song, W.; Chen, L.; Ma, S.; Deng, J.; Zheng, H.; Li, Y.; Liu, J.; Zhao, Z. Density functional theory study of the formaldehyde catalytic oxidation mechanism on a Au-doped CeO₂(111) surface. *J. Phys. Chem. C* **2018**, *122*, 438–448. [[CrossRef](#)]
25. Liu, B.; Liu, Y.; Li, C.; Hu, W.; Jing, P.; Wang, Q.; Zhang, J. Three dimensionally ordered macroporous Au/CeO₂-Co₃O₄ catalysts with nanoporous walls for enhanced catalytic oxidation of formaldehyde. *Appl. Catal. B Environ.* **2012**, *127*, 47–58. [[CrossRef](#)]
26. Lu, S.; Wang, F.; Chen, C.; Huang, F.; Li, K. Catalytic oxidation of formaldehyde over CeO₂-Co₃O₄ catalysts. *J. Rare Earths* **2017**, *35*, 867–874. [[CrossRef](#)]
27. Qu, J.; Chen, D.; Li, N.; Xu, Q.; Li, H.; He, J.; Lu, J. 3D gold-modified cerium and cobalt oxide catalyst on a graphene aerogel for highly efficient catalytic formaldehyde oxidation. *Small* **2018**, *15*, 1804415. [[CrossRef](#)] [[PubMed](#)]
28. Rochard, G.; Giraudon, J.M.; Liotta, L.F.; La Parola, V.; Lamonier, J.F. Au/Co promoted CeO₂ catalysts for formaldehyde total oxidation at ambient temperature: Role of oxygen vacancies. *Catal. Sci. Technol.* **2019**, *9*, 3203–3213. [[CrossRef](#)]
29. Ilieva, L.; Petrova, P.; Venezia, A.M.; Anghel, E.M.; State, R.; Avdeev, G.; Tabakova, T. Mechanochemically prepared Co₃O₄-CeO₂ catalysts for complete benzene oxidation. *Catalysts* **2021**, *11*, 1316. [[CrossRef](#)]
30. Haneda, M.; Kintaichi, Y.; Bion, N.; Hamada, H. Alkali metal-doped cobalt oxide catalysts for NO decomposition. *Appl. Catal. B Environ.* **2003**, *46*, 473–482. [[CrossRef](#)]
31. Ma, L.; Seo, C.Y.; Chen, X.; Li, J.; Schwank, J.W. Sodium-promoted Ag/CeO₂ nanospheres for catalytic oxidation of formaldehyde. *Chem. Eng. J.* **2018**, *350*, 419–428. [[CrossRef](#)]
32. Reina, T.R.; Ivanova, S.; Delgado, J.J.; Ivanov, I.; Idakiev, V.; Tabakova, T.; Centeno, M.A.; Odriozola, J.A. Viability of Au/CeO₂-ZnO/Al₂O₃ catalysts for pure hydrogen production by the water-gas shift reaction. *ChemCatChem* **2014**, *6*, 1401–1409.
33. Gabrovska, M.; Ivanov, I.; Nikolova, D.; Kovacheva, D.; Tabakova, T. Hydrogen production via water-gas shift reaction over gold supported on Ni-based layered double hydroxides. *Int. J. Hydrogen Energy* **2021**, *46*, 458–473. [[CrossRef](#)]
34. Liu, Q.; Wang, L.C.; Chen, M.; Cao, Y.; He, H.Y.; Fan, K.N. Dry citrate-precursor synthesized nanocrystalline cobalt oxide as highly active catalyst for total oxidation of propane. *J. Catal.* **2009**, *263*, 104–113. [[CrossRef](#)]
35. Liu, Y.; Dai, H.; Deng, J.; Xie, S.; Yang, H.; Tan, W.; Han, W.; Jiang, Y.; Guo, G. Mesoporous Co₃O₄-supported gold nanocatalysts: Highly active for the oxidation of carbon monoxide, benzene, toluene, and o-xylene. *J. Catal.* **2014**, *309*, 408–418. [[CrossRef](#)]
36. Laguna, O.H.; Sarria, F.R.; Centeno, M.A.; Odriozola, J.A. Gold supported on metal-doped ceria catalysts (M = Zr, Zn and Fe) for the preferential oxidation of CO (PROX). *J. Catal.* **2010**, *276*, 360–370. [[CrossRef](#)]
37. Shoko, E.; Smith, M.F.; McKenzie, R.H. Charge Distribution near bulk oxygen vacancies in cerium oxides. *J. Phys. Condens. Matter* **2010**, *22*, 223201. [[CrossRef](#)]
38. Wang, H.; Zhu, H.; Qin, Z.; Wang, G.; Liang, F.; Wang, J. Preferential oxidation of CO in H₂ rich stream over Au/CeO₂-Co₃O₄ catalysts. *Catal. Commun.* **2008**, *9*, 1487–1492. [[CrossRef](#)]
39. Ilieva, L.; Petrova, P.; Pantaleo, G.; Zanella, R.; Sobczak, J.W.; Lisowski, W.; Kaszukur, Z.; Munteanu, G.; Yordanova, I.; Liotta, L.F.; et al. Alumina supported Au/Y-doped ceria catalysts for pure hydrogen production via PROX. *Int. J. Hydrogen Energy* **2019**, *44*, 233–245. [[CrossRef](#)]
40. Chen, B.; Zhu, X.; Wang, Y.; Yu, L.; Shi, C. Gold stabilized on various oxide supports catalyzing formaldehyde oxidation at room temperature. *Chin. J. Catal.* **2016**, *37*, 1729–1737. [[CrossRef](#)]
41. Yao, Y.F.Y. The oxidation of hydrocarbons and CO over metal oxides: III. Co₃O₄. *J. Catal.* **1974**, *33*, 108–122. [[CrossRef](#)]

42. Yao, H.C.; Yao, Y.F.Y. Ceria in automotive exhaust catalysts: I. Oxygen storage. *J. Catal.* **1984**, *86*, 254–265. [[CrossRef](#)]
43. Zou, G.; Xu, Y.; Wang, S.; Chen, M.; Shangguan, W. The synergistic effect in Co-Ce oxides for catalytic oxidation of diesel soot. *Catal. Sci. Technol.* **2015**, *5*, 1084–1092. [[CrossRef](#)]
44. Deng, J.; Song, W.; Chen, L.; Wang, L.; Jing, M.; Ren, Y.; Zhao, Z.; Liu, J. The effect of oxygen vacancies and water on HCHO catalytic oxidation over Co₃O₄ catalyst: A combination of density functional theory and microkinetic study. *Chem. Eng. J.* **2019**, *355*, 540–550. [[CrossRef](#)]
45. Andreeva, D.; Idakiev, V.; Tabakova, T.; Ilieva, L.; Falaras, P.; Bourlinos, A.; Travlos, A. Low-temperature water-gas shift reaction over Au/CeO₂ catalysts. *Catal. Today* **2002**, *72*, 51–57. [[CrossRef](#)]
46. Liotta, L.F.; Pantaleo, G.; Puleo, F.; Venezia, A.M. Au/CeO₂-SBA-15 catalysts for CO oxidation: Effect of ceria loading on physicochemical properties and catalytic performances. *Catal. Today* **2012**, *187*, 10–19. [[CrossRef](#)]
47. Balzer, R.; Probst, L.F.D.; Drago, V.; Schreiner, W.H.; Fajardo, H.V. Catalytic oxidation of volatile organic compounds (n-hexane, benzene, toluene, o-xylene) promoted by cobalt catalysts supported on γ -Al₂O₃-CeO₂. *Braz. J. Chem. Eng.* **2014**, *31*, 757–769. [[CrossRef](#)]
48. Biesinger, M.C.; Payne, B.P.; Grosvenor, A.P.; Lau, L.W.M.; Gerson, A.R.; Smart, R.S.C. Resolving surface chemical states in XPS analysis of first row transition metals, oxides and hydroxides: Cr, Mn, Fe, Co and Ni. *Appl. Surf. Sci.* **2011**, *257*, 2717–2730. [[CrossRef](#)]
49. Wang, J.; Yoshida, A.; Wang, P.; Yu, T.; Wang, Z.; Hao, X.; Abudula, A.; Guan, G. Catalytic oxidation of volatile organic compound over cerium modified cobalt-based mixed oxide catalysts synthesized by electrodeposition method. *Appl. Catal. B Environ.* **2020**, *271*, 118941. [[CrossRef](#)]
50. Kang, M.; Song, M.W.; Lee, C.H. Catalytic carbon monoxide oxidation over CoOx/CeO₂ composite catalysts. *Appl. Catal. A Gen.* **2003**, *251*, 143–156. [[CrossRef](#)]
51. Xue, L.; Zhang, C.; He, H.; Teraoka, Y. Catalytic decomposition of N₂O over CeO₂ promoted Co₃O₄ spinel catalyst. *Appl. Catal. B Environ.* **2007**, *75*, 167–174. [[CrossRef](#)]
52. Sun, M.; Wang, L.; Feng, B.; Zhang, Z.; Lu, G.; Guo, Y. The role of potassium in K/Co₃O₄ for soot combustion under loose contact. *Catal. Today* **2011**, *175*, 100–105. [[CrossRef](#)]
53. Ismail, A.; Li, M.; Zahid, M.; Fan, L.; Zhang, C.; Li, Z.; Zhu, Y. Effect of strong interaction between Co and Ce oxides in Co_xCe_{1-x}O_{2- δ} oxides on its catalytic oxidation of toluene. *Mol. Catal.* **2021**, *502*, 111356. [[CrossRef](#)]
54. Dang-Bao, T.; Anh, N.P.; Phuong, P.H.; Van, N.T.T.; Nghia, T.N.D.; Tien, H.V.; Tri, N. Fabrication of cobalt-doped ceria nanorods for p-xylene deep oxidation: Effects of cobalt precursor and loading. *Mater. Trans.* **2020**, *61*, 1294–1300. [[CrossRef](#)]
55. Li, X.; Li, X.; Zeng, X.; Zhu, T. Correlation between the physicochemical properties and catalytic performances of micro/mesoporous CoCeOx mixed oxides for propane combustion. *Appl. Catal. A Gen.* **2019**, *572*, 61–70. [[CrossRef](#)]
56. Ma, C.; Mu, Z.; He, C.; Li, P.; Li, J.; Hao, Z. Catalytic oxidation of benzene over nanostructured porous Co₃O₄-CeO₂ composite catalysts. *J. Environ. Sci.* **2011**, *23*, 2078–2086. [[CrossRef](#)]
57. Casaletto, M.P.; Longo, A.; Martorana, A.; Prestianni, A.; Venezia, A.M. XPS study of supported gold catalysts: The role of Au⁰ and Au^{+ δ} species as active sites. *Surf. Interface Anal.* **2006**, *38*, 215–218. [[CrossRef](#)]
58. Jia, M.L.; Bai, H.F.; Zhaorigetu; Shen, Y.N.; Li, Y.F. Preparation of Au/CeO₂ catalyst and its catalytic performance for HCHO oxidation. *J. Rare Earths* **2008**, *26*, 528–531. [[CrossRef](#)]
59. Li, H.F.; Zhang, N.; Chen, P.; Luo, M.F.; Lu, J.Q. High surface area Au/CeO₂ catalysts for low temperature formaldehyde oxidation. *Appl. Catal. B Environ.* **2011**, *110*, 279–285. [[CrossRef](#)]
60. Chen, B.B.; Shi, C.A.; Crocker, M.; Wang, Y.; Zhu, A.M. Catalytic removal of formaldehyde at room temperature over supported gold catalysts. *Appl. Catal. B Environ.* **2013**, *132*, 245–255. [[CrossRef](#)]
61. Bu, Y.; Chen, Y.; Jiang, G.; Hou, X.; Li, S.; Zhang, Z. Understanding of Au-CeO₂ interface and its role in catalytic oxidation of formaldehyde. *Appl. Catal. B Environ.* **2020**, *260*, 118138. [[CrossRef](#)]
62. Lou, Y.; Ma, J.; Cao, X.; Wang, L.; Dai, Q.; Zhao, Z.; Cai, Y.; Zhan, W.; Guo, Y.; Hu, P.; et al. Promoting effects of In₂O₃ on Co₃O₄ for CO oxidation: Tuning O₂ activation and CO adsorption strength simultaneously. *ACS Catal.* **2014**, *4*, 4143–4152. [[CrossRef](#)]
63. Sun, Y.; Gao, S.; Lei, F.; Liu, J.; Liang, L.; Xie, Y. Atomically-thin nonlayered cobalt oxide porous sheets for highly efficient oxygen evolving electrocatalysts. *Chem. Sci.* **2014**, *5*, 3976–3982. [[CrossRef](#)]
64. Yu, J.; Li, X.; Xu, Z.; Xiao, W. NaOH-modified ceramic honeycomb with enhanced formaldehyde adsorption and removal performance. *Environ. Sci. Technol.* **2013**, *47*, 9928–9933. [[CrossRef](#)] [[PubMed](#)]
65. Chen, B.B.; Zhu, X.B.; Crocker, M.; Wang, Y.; Shi, C. Complete oxidation of formaldehyde at ambient temperature over γ -Al₂O₃ supported Au catalyst. *Catal. Commun.* **2013**, *42*, 93–97. [[CrossRef](#)]
66. Bortolotti, M.; Lutterotti, L.; Lonardelli, I. ReX: A computer program for structural analysis using powder diffraction data. *J. Appl. Cryst.* **2009**, *42*, 538–539. [[CrossRef](#)]
67. Kotzev, N.; Shopov, D. A thermodesorption study of the system olefin–NiO. *J. Catal.* **1971**, *22*, 297–301. [[CrossRef](#)]
68. Monti, D.A.M.; Baiker, A. Temperature-programmed reduction, parametric sensitivity and estimation of kinetic parameters. *J. Catal.* **1983**, *83*, 323–335. [[CrossRef](#)]
69. Venezia, A.M.; Murania, R.; Pantaleo, G.; Deganello, G. Pd and PdAu on mesoporous silica for methane oxidation: Effect of SO₂. *J. Catal.* **2007**, *251*, 94–102. [[CrossRef](#)]